ISSN 1674-1056
http://cpb.iphy.ac.cn
http://iopscience.iop.org/cpb
中国物理 B
Chinese Physics
中国物理 Chinese Physics B

Black phosphorus-based field effect transistor devices for Ag ions detection

Hui-De Wang(王慧德), David K Sang, Zhi-Nan Guo(郭志男), Rui Cao(曹睿), Jin-Lai Zhao(赵劲来), Muhammad Najeeb Ullah Shah, Tao-Jian Fan(范涛健), Dian-Yuan Fan(范滇元), Han Zhang(张晗)

Citation: Chin. Phys. B . 2018, 27(8): 087308. **doi:** 10.1088/1674-1056/27/8/087308

Journal homepage: http://cpb.iphy.ac.cn; http://iopscience.iop.org/cpb

What follows is a list of articles you may be interested in

Intrinsic charge transport behaviors in graphene-black phosphorus van der Waals heterojunction devices

Guo-Cai Wang(王国才), Liang-Mei Wu(吴良妹), Jia-Hao Yan(严佳浩), Zhang Zhou(周璋), Rui-Song Ma(马瑞松), Hai-Fang Yang(杨海方), Jun-Jie Li(李俊杰), Chang-Zhi Gu(顾长志), Li-Hong Bao(鲍丽宏), Shi-Xuan Du(杜世萱), Hong-Jun Gao(高鸿钧)

Chin. Phys. B . 2018, 27(7): 077303. **doi:** 10.1088/1674-1056/27/7/077303

Enhanced transient photovoltaic characteristics of core-shell ZnSe/ZnS/L-Cys quantum-dot-sensitized TiO_2 thin-film

Kui-Ying Li(李葵英), Lun Ren(任伦), Tong-De Shen(沈同德)

Chin. Phys. B . 2018, 27(6): 067305. **doi:** 10.1088/1674-1056/27/6/067305

Electronic transport properties of Co cluster-decorated graphene

Chao-Yi Cai(蔡超逸), Jian-Hao Chen(陈剑豪)

Chin. Phys. B . 2018, 27(6): 067304. **doi:** 10.1088/1674-1056/27/6/067304

Closed-form internal impedance model and characterization of mixed carbon nanotube bundles for three-dimensional integrated circuits

Qijun Lu(卢启军), Zhangming Zhu(朱樟明), Yintang Yang(杨银堂), Ruixue Ding(丁瑞雪), Yuejin Li(李跃进)

Chin. Phys. B . 2018, 27(1): 017303. **doi:** 10.1088/1674-1056/27/1/017303

Toward high-performance two-dimensional black phosphorus electronic and optoelectronic devices

Xuefei Li(李学飞), Xiong Xiong(熊雄), Yanqing Wu(吴燕庆)

Chin. Phys. B . 2017, 26(3): 037307. **doi:** 10.1088/1674-1056/26/3/037307

SPECIAL TOPIC — Nanophotonics

Black phosphorus-based field effect transistor devices for Ag ions detection*

Hui-De Wang(王慧德)[1], David K Sang[1], Zhi-Nan Guo(郭志男)[1,†], Rui Cao(曹睿)[1,2], Jin-Lai Zhao(赵劲来)[2], Muhammad Najeeb Ullah Shah[1], Tao-Jian Fan(范涛健)[1], Dian-Yuan Fan(范滇元)[1], and Han Zhang(张晗)[1,‡]

[1] *Shenzhen Key Laboratory of Two-Dimensional Materials and Devices, Shenzhen Engineering Laboratory of Phosphorene and Optoelectronics, SZU-NUS Collaborative Innovation Center for Optoelectronic Science & Technology, College of Optoelectronic Engineering, Shenzhen University, Shenzhen* 518060, *China*

[2] *Faculty of Information Technology, Macau University of Science and Technology, Macao, China*

(Received 29 April 2018; revised manuscript received 21 May 2018; published online 25 July 2018)

Black phosphorus (BP), an attractive two-dimensional (2D) semiconductor, is widely used in the fields of optoelectronic devices, biomedicine, and chemical sensing. Silver ion (Ag^+), a commonly used additive in food industry, can sterilize and keep food fresh. But excessive intake of Ag^+ will harm human health. Therefore, high sensitive, fast and simple Ag^+ detection method is significant. Here, a high-performance BP field effect transistor (FET) sensor is fabricated for Ag^+ detection with high sensitivity, rapid detection speed, and wide detection concentration range. The detection limit for Ag^+ is 10^{-10} mol/L. Testing time for each sample by this method is 60 s. Besides, the mechanism of BP-FET sensor for Ag^+ detection is investigated systematically. The simple BP-FET sensor may inspire some relevant research and potential applications, such as providing an effective method for the actual detection of Ag^+, especially in witnessed inspections field of food.

Keywords: black phosphorus, semiconductor devices, chemical sensing, witnessed inspections

PACS: 73.63.–b, 85.30.Tv, 07.07.Df **DOI:** 10.1088/1674-1056/27/8/087308

1. Introduction

Black phosphorus (BP) is a new type of two-dimensional (2D) semiconducting material with a direct bandgap that changes with its thickness.[1–5] Few-layer BP has excellent electrical transport properties, such as high carrier mobility (10^4 $cm^2 \cdot V^{-1} \cdot s^{-1}$) and large current on/off ratio (1×10^5 [6–9] Additional, BP shows prominent in-plane anisotropic electrical characteristics, which origin from its honeycomb structure,[10] quantum transport characteristics of carriers,[11] and excellent optical-response properties.[2,12–19] Because of these attractive properties, BP has been regarded as a promising material for applications in (photo) electronic devices, phototherapy, thermoelectric devices and sensors.[20–41] However, the instability of BP under ambient conditions affects its practical applications.[42–46] Previous study shows that metal ion can be modified on BP surface via the cation–π interaction to enhance both the ambient stability and transport properties of BP. Among the metal ions, Ag^+ shows a relatively high binding energy with BP, which is 41.8 eV.[47] Such a strong binding energy and the transport properties enhancement effect give BP-FET device a new application direction, Ag^+ detection.

Ag^+ ion, a heavy metal ion, has outstanding bactericidal performance because it can be combined with the sulfhydryl (–SH) in the bacteria, leading to the inactivation of the protease in the bacteria with –SH as an active unit. Of all the metal ions, Ag^+ ion has the second highest bactericidal activity and Hg^{2+} ion has the highest bactericidal activity but it is toxic. Therefore, Ag^+ ion is widely used as food functional additives. However, human protease activity can also be suppressed by high concentration of Ag^+ ions, and excessive Ag^+ ions entering into human body through food will seriously harm human health.[48,49] Therefore, it is very important to detect and control the residual of Ag^+ ions in food. Different detection methods will be used for Ag^+ ions indifferent samples, such as atomic absorption spectrometry (AAS),[50] inductively coupled plasma (ICP),[51–53] etc. Although these methods are accurate enough for quantitatively analysing the Ag^+ ions in the samples, high cost, time-consuming, and complicated instrumentations are the main factors hindering their applications for fast *in-situ* detection.

In this work, the detection of Ag^+ in N-methyl pyrrolidone (NMP) solution is first realized by the BP-FET sensor through the cation–π interaction between Ag^+ and BP.

*Project support by the National Natural Science Foundation of China (Grant Nos. 61605131 and 61435010) and the Shenzhen Science and Technology Research Fund, China (Grant No. JCYJ20150324141711624).

†Corresponding author. E-mail: guozhinan@szu.edu.cn

‡Corresponding author. E-mail: hzhang@szu.edu.cn

© 2018 Chinese Physical Society and IOP Publishing Ltd

The detection limit for Ag^+ by the BP-FET chip method is 10^{-10} mol/L(0.01 ppb), which is below the allowable limit concentration (0.1 ppm) of Ag^+ ions in drinking water specified by the World Health Organization (WHO). And the detection time for each sample is 60 s. Finally, the mechanism of BP-FET sensor for Ag^+ detection is investigated. Such a simple BP-FET sensor can provide an effective way for actual detection of Ag^+, especially in witnessed inspections field of food.

2. Experiment

2.1. Materials

The BP crystals ($\geq 99.999\%$) were obtained from Smart–Elements and stored in a vacuum drying chamber. Silver nitrate (analytical reagent grade) was purchased from SigmaAldrich (Santa Barbara, CA, USA). NMP ($\geq 99.5\%$, analytical reagent grade, anhydrous) was purchased from Aladdin Reagents, and acetone ($\geq 99.5\%$, analytical reagent grade, anhydrous) was purchased from Casmart.

2.2. Sample preparation

BP-FET sensor preparation process is as follows. Few-layer BP films were obtained from bulk BP crystals by mechanical exfoliation with scotch tape and then were transferred to an Si/SiO_2 (300 nm) substrate with a poly(dimethyl siloxane) (PDMS) thin film as a medium. The sample thickness was determined by an optical microscope and an atomic force microscope. The BP sheets on the Si/SiO_2 (300 nm) substrate were spin-coated with methyl methacrylate (MMA) and poly(methyl methacrylate) (PMMA) and dried at 100 °C by heating plate for 60 s and 120 s, respectively. Electron-beam lithography (EBL, FEI Nova Nano SEM 450 with NPGS system) was used to define the position and shape of drain and source electrodes. The drain and source electrodes were fabricated by electron beam evaporator (DE400EVP). Finally, BP-FET sensor was obtained by the lift-off process with acetone.

Silver ion adsorption process is as follows. BP-FET sensor was soaked in the NMP solution containing the Ag^+ ions for different times and different concentrations. Then, the device was removed, washed with NMP, and dried with nitrogen rapidly.

2.3. Characterization

The topographies and thickness values of BP sheets were obtained from atomic force microscopy (AFM, Bruker) in the standard tapping mode. Raman scattering was obtained from the Horiba Jobin–YvonLabRam HR-VIS high-resolution confocal Raman microscope equipped with a 633-nm laser as the excitation source and an XYZ motorized sample stage controlled by LabSpec software. The laser spot size on the surface of the sample was about 1 μm after being focused by a 50× objective lens with a numerical aperture of 0.90. Electrical properties of the BP-FET sensor were tested by Keithley 4200 semiconductor characteristic analyzer system (Keithley, 4200 SCS) combined with a probe station in air.

3. Results and discussion

Figure 1 is a schematic diagram of BP-FET sensor preparation and testing process. The device preparation process consists of five steps. Firstly, few-layer BP sheets were obtained by mechanical exfoliation with scotch tape and then were transferred onto the surface of Si/SiO_2 (300 nm) substrate by a PDMS thin film as a medium. Secondly, the sample thickness was determined by an optical microscope and an atomic force microscope. Thirdly, the sample on the Si/SiO_2 (300 nm) substrate was spin-coated with MMA and PMMA and dried by heating plate, respectively. Then, EBL, developing processes and electron beam evaporator of semiconductor processes were used to define the position and shape of drain and source electrodes. Finally, the BP-FET sensor was obtained after lift-off process with acetone whose typical electrodes were made up of chromium (5 nm in thickness) and gold (40 nm in thickness). The silicon substrate whose surface oxide was partially removed by the silicon blade was used as the back-gate electrode.

Sequentially, the device testing process consists of three steps. Firstly, BP-FET sensor was soaked in NMP solution containing Ag^+ ions for different times and different concentrations. Then, the device was removed, washed with NMP, and dried with nitrogen rapidly. Finally, electrical properties of the BP- FET sensor were tested by Keithley 4200 semiconductor characteristic analyzer system combined with a probe station in air.

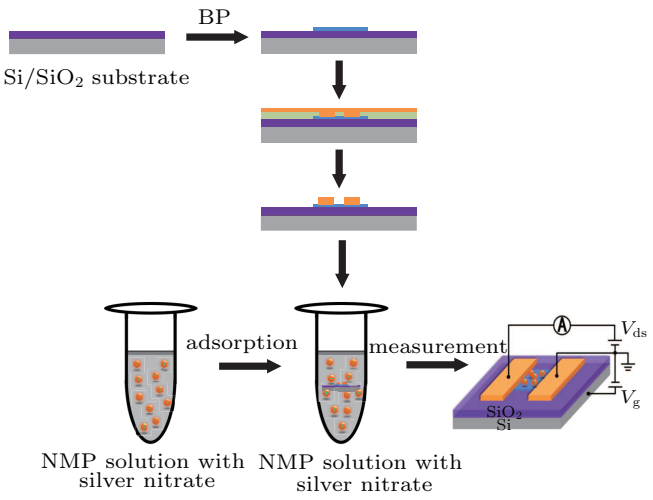


Fig. 1. (color online) Schematic diagram of fabrication, Ag^+ adsorption and measurement process of BP-FET sensor.

Typical BP films each with a thickness of less than 30 nm are selected through an optical microscope by optical contrast

identification. The exact thickness of BP sheets is determined by AFM. Figure 2(a) shows surface topographic image of a BP sheet obtained from AFM with standard tapping mode. Height image of BP sample as shown in Fig. 2(b), indicates that the thickness is about 10 nm. Figure 2(c) shows the Raman scattering spectra obtained from a BP sheet adsorbed Ag^+ ($BP_{Ag(+)}$) and a pristine BP sheet, respectively. Each spectrum shows three characteristic peaks at $\sim 369\ cm^{-1}$, $\sim 438\ cm^{-1}$, and $\sim 466\ cm^{-1}$, which corresponds to the A_g^1, B_{2g}, and A_g^2 vibrational modes of P in BP.[23,54–56] The A_g^1 peak corresponds to the vibrational mode of out-of-plane, and B_{2g} and A_g^2 peaks correspond to the vibrational modes of in-plane. The selective enhancement of the A_g^1 peak (as shown in Fig. 2(c)) indicates that the Ag^+ ions are successfully adsorbed on the surface of the BP sheet.

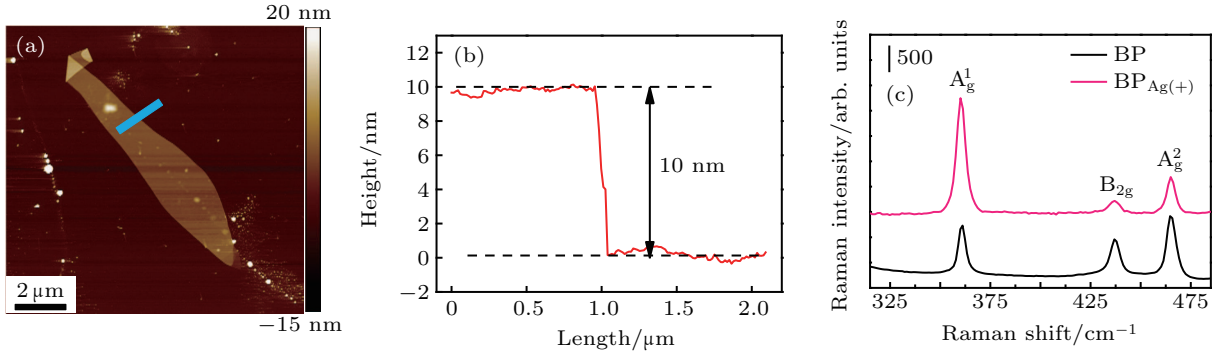


Fig. 2. (color online) (a) AFM topographic image of BP sheet. (b) AFM height profile of BP sheet obtained from panel (a), demonstrating a height of about 10 nm. (c) Raman spectra of BP sheet and $BP_{Ag(+)}$ sheet.

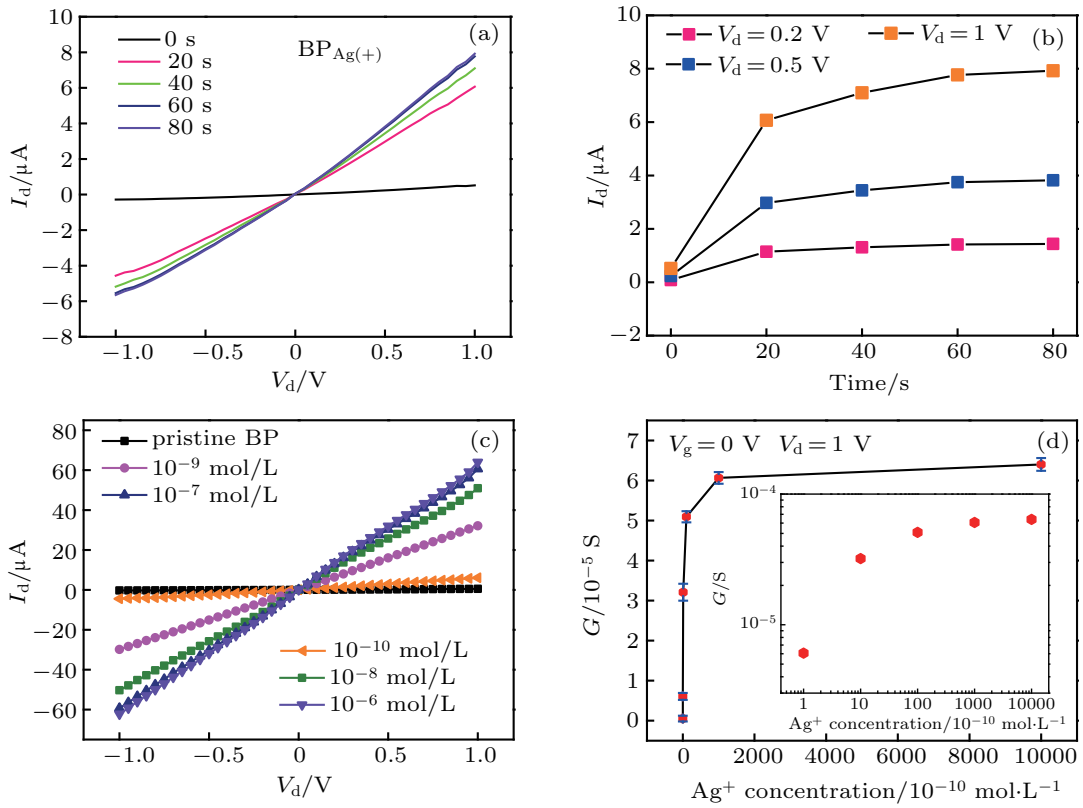


Fig. 3. (color online) (a)I_{ds} versus V_{ds} curves obtained from the BP-FET after Ag^+ adsorption for 0 s, 20 s, 40 s, 60 s, 80 s. $V_{gs} = 0$ V. (b) I_{ds} versus adsorption–time curves obtained from panel (a), at $V_d = 0.2$ V, 0.5 V, and 1.0 V, respectively. (c) I_{ds} versus V_{ds} curves obtained from the BP-FET after Ag^+ adsorption for 60 s with different Ag^+ concentrations ranging from 10^{-10} mol/L to 10^{-6} mol/L at room temperature, $V_{gs} = 0$ V. (d) Conductance versus ion concentrations curves obtained from panel (c), at $V_{ds} = 1.0$ V, $V_{gs} = 0$ V (inset: logarithmic scale).

After the BP-FET sensor is prepared, the Ag^+ adsorption time dependence and Ag^+ adsorption concentration dependence of the device were studied by Keithley 4200 semiconductor characteristic analyzer system (Keithley, 4200SCS), and the results are shown in Fig. 3.

A BP-FET sensor is soaked in NMP solution for 0 s, 20 s, 40 s, 60 s, 80 s, separately, of which the Ag^+ concentration is 10^{-10} mol/L. Then, the source–drain current I_{ds} ver-

sus source–drain voltage V_{ds} characteristics for different Ag^+ adsorption time are obtained as shown in Fig. 3(a). The back-gate voltage V_{gs} is 0 V. The Ag^+ adsorption time dependence current–time curves obtained from Fig. 3(a), with $V_d = 0.2$ V, 0.5 V, and 1.0 V, respectively,indicate that the current increases with the adsorption time of Ag^+ ions increasing. After the adsorption time is greater than 60 s, the increasing current becomes saturated as shown in Fig. 3(b). It implies that the detection time is only 60 s. However, the thickness of the BP directly affects the sensing performance of the device. As shown in Fig. S5 in Appendix A, the sensing characteristics of the device on thin BP (3 nm–5 nm) are fairly good, but its own performance is unstable, which is not suitable for accurately Ag^+ detection. For the devices on thick BP ($\sim$ 20 nm), the sensing performance is not good. In this case, we choose the BP with a thickness of around 10 nm for the FET device fabrication.

After BP-FET sensor is soaked in NMP solution for 60 s, with different Ag^+ ion concentrations ranging from 10^{-10} mol/L to 10^{-6} mol/L at room temperature, the source–drain current I_{ds} versus source–drain voltage V_{ds} characteristics are investigated as shown in Fig. 3(c). The back-gate voltage V_{gs} is set to be 0 V. The Ag^+ ion concentration-dependent current curves obtained from Fig. 3(c), with $V_d = 1.0$ V, indicates that the conductance increases with the concentration of Ag^+ ions increasing. After the concentration of Ag^+ ions is larger than 10^{-6} mol/L, the increasing conductance becomes saturated as shown in Fig. 3(d) (inset: logarithmic scale). It implies that the concentration detection capability of BP-FET sensor for Ag^+ ions ranges from 10^{-10} mol/L to 10^{-6} mol/L. For the Ag^+ sample with a concentration of 10^{-11} mol/L, the device cannot well work as a sensing medium, even the adsorption time for Ag^+ is extended to 10 min as shown in Fig. S6 in Appendix A.

The sensing mechanism of BP-FET sensor is investigated systematically. The conductance of BP can be expressed as the following formula:

$$\sigma = nq\mu,$$

where σ is the conductance, n is the carrier concentration, q is the charge per carrier, μ is the carrier mobility, and q is a constant. So, the conductance is related to carrier concentration and carrier mobility.

Figure 4(a) is the output curve of the BP-FET device before and after Ag^+ adsorption, in which the adsorption time is 60 s and the Ag^+ concentration is 10^{-10} mol/L at $V_{gs} = 0$ V. Figure 4(b) shows the transfer curve of the BP-FET device before and after Ag^+ adsorption under the same conditions, at $V_{ds} = 0.5$ V. The channel length and width of the device are typically 3 μm and 3 μm, respectively. So, according to the formula of carrier mobility[1]

$$\mu = \frac{1}{C_i}\frac{L}{W}\frac{dI_{ds}}{dV_{gs}}\frac{1}{V_{ds}},$$

where C_i is the back-gate oxide capacitance per unit area ($C_i = \varepsilon_0\varepsilon_r/d$; $\varepsilon_r = 3.9$ for SiO_2; d is the thickness of SiO_2 layer, which is 300 nm), L and W are the length and width of BP-FET sensor, respectively. Carrier mobility is 297 $cm^2 \cdot V^{-1} \cdot s^{-1}$ and 432 $cm^2 \cdot V^{-1} \cdot s^{-1}$ before and after adsorption Ag^+, respectively, which could be calculated from Fig. 4(b). It is just less than twice quantitative relation while the conductance is almost twelve times quantitative relation obtained from Fig. 4(a). It indicates that the dominant factor for the increase of BP conductance during BP-FET sensing Ag^+ ions is the change of carrier concentration rather than the change of carrier mobility.

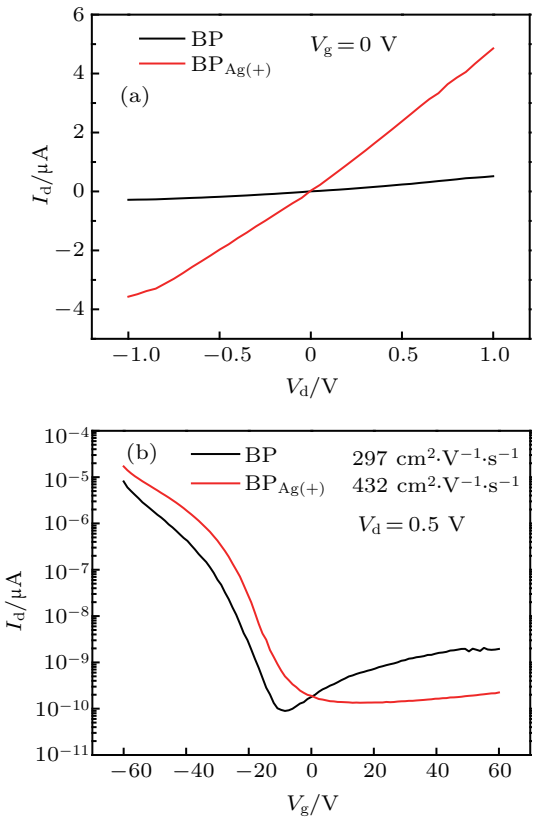


Fig. 4. (color online) (a) Output and (b) transfer curves of BP-FET sensor before (black) and after (red) Ag^+ adsorption (10^{-10} mol/L, 60 s), with channel length and width of the device being both 3 μm.

We continue to explore the process of Ag^+ adsorption on the BP surface. Concretely, Ag^+ ion interacts with the conjugated π bond, which derives from the lone pair electrons of the phosphorus atoms in surface layer, via the cation–π interaction, as shown in Fig. 5(a).[47] BP is a p-type semiconductor with adjustable band gap, so its majority carriers are holes and its Fermi energy is close to the conduction band. The Ag^+ ion adsorption acts as a negative back-gate voltage on the surface of BP sheet because of the positive characteristic of Ag^+ ions,

which will inject additional holes into BP sheet. As a result, Fermi level (E_F) of BP sheet will move close to the valence band as shown in Fig. 5(b), which will increase hole concentration in BP sheet and then increase its conductance.Beside Ag^+ ions, other kinds of metal ions like Mg^{2+} and Fe^{3+} can also be adsorbed on the surface of BP working as an additional hole medium and enhance the p-type transport performance of the devices as shown in Fig. S7 in Appendix A.

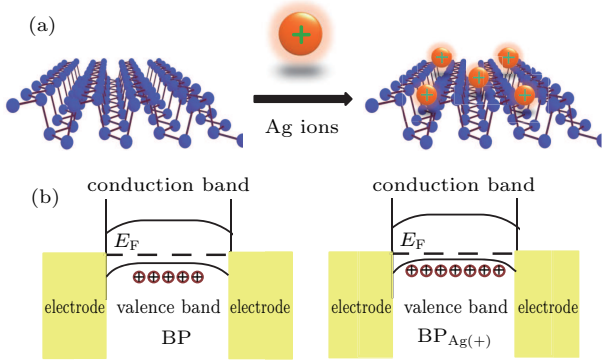


Fig. 5. (color online) (a) Schematic of Ag^+ adsorption to the surface of BP-FET. (b) Band structure of BP before and after Ag^+ absorption. It shows that Fermi level of BP sheets moves close to valence band, increasing hole concentration and conductance of BP sheet because of Ag^+ absorption.

4. Conclusions

In this research, a high-performance BP-FET sensor for Ag^+ detection with high sensitivity, rapid detection speed and wide concentration detection range has been fabricated by micro-nano machining. Based on the BP-FET sensor, the detection limit for Ag^+ can reach 10^{-10} mol/L ($\sim$ 0.01 ppb), which is far below the allowable limit concentration (0.1 ppm) of Ag^+ in drinking water. The detection time is 1 min for each sample. The reason why BP-FET can be used for Ag^+ detection is the cation–π interactions between Ag^+ and BP. When Ag^+ ions attach on the surface of BP, which equivalent to introducing plenty of holes into a bipolar semiconductor, the p-type transport behavior of the device will be enhanced. The BP-FET sensor shows a new application direction of FETs and provides an effective method for the actual detection of Ag^+, especially in witnessed inspections field of food.

Appendix A: Supporting information

In order to better understand our studies of the the present article, some figures are provided in the following part.

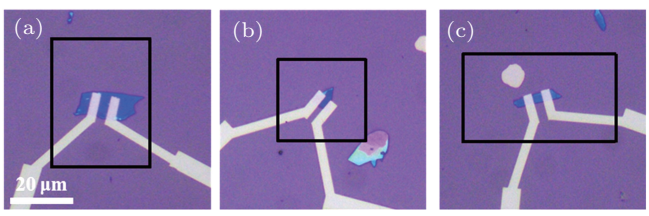


Fig. S1. (color online) Microphotographs of typical BP sheets on the surface of the Si/SiO_2 (300 nm) substrate.

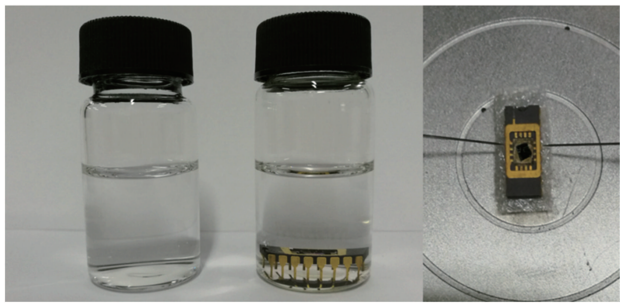


Fig. S2. (color online) Schematic diagram of Ag^+ adsorption and electrical test of BP-FET sensor.

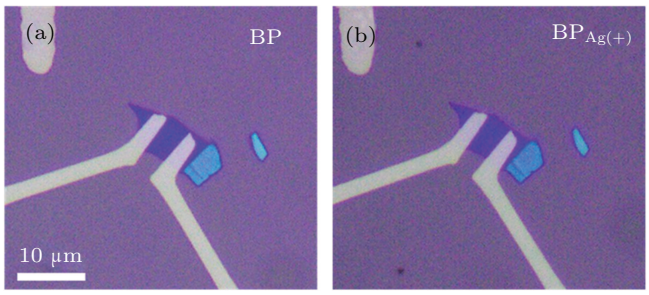


Fig. S3. (color online) Microphotographs of typical BP sheets before and after Ag^+ adsorption on the surface of the Si/SiO_2 (300 nm) substrate.

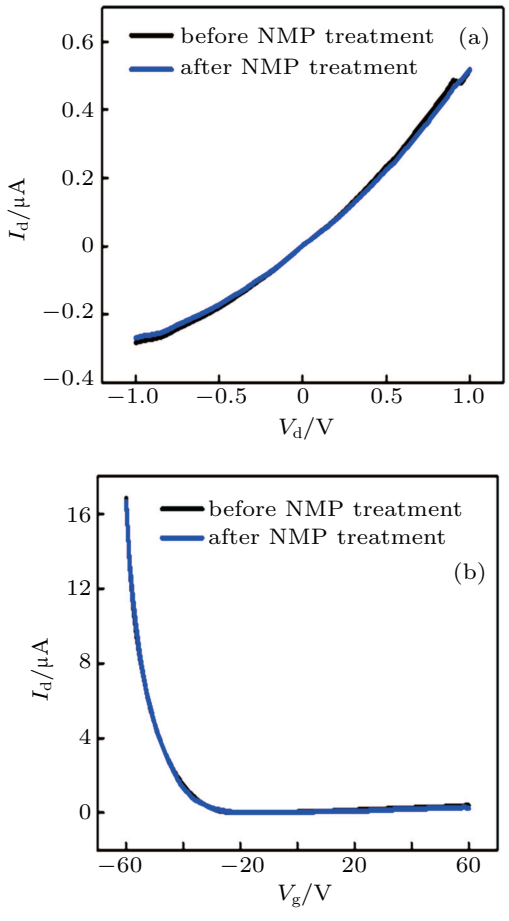


Fig. S4. (color online) I_{ds}–V_{ds} curve (a) and I_{ds}–V_{gs} curve (b) obtained from the BP-FET device on the Si/SiO_2 (300 nm) substrate before and after treatment with pure NMP for 60 s.

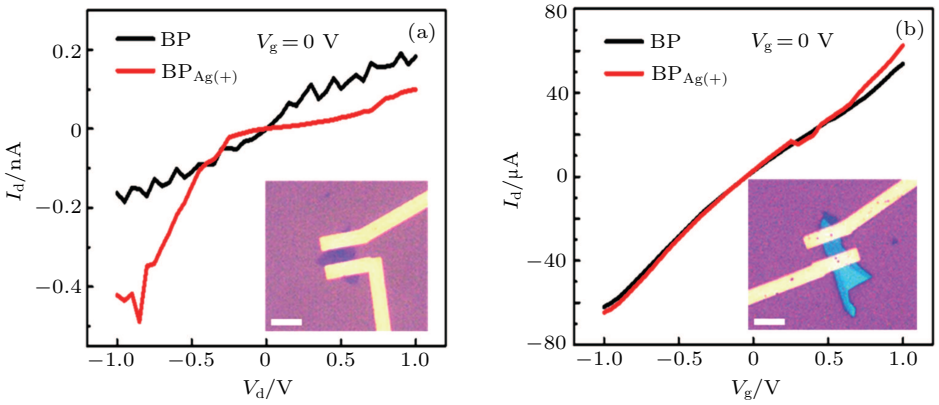


Fig. S5. (color online) I_{ds}–V_{ds} curve obtained from the thin (a) and thick (b) BP-FET devices on the Si/SiO_2 (300 nm) substrate before and after Ag^+ adsorption for 60 s with concentration of 10^{-10} mol/L (inset: optical picture of BP-FET device, the scale bar is 6 μm).

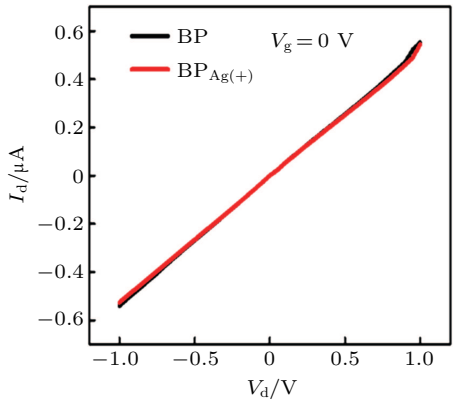


Fig. S6. (color online) I_{ds}–V_{ds} curve obtained from BP-FET device on the Si/SiO_2 (300 nm) substrate before and after Ag^+ adsorption for 10 min with concentration of 10^{-11} mol/L, at $V_g = 0$ V.

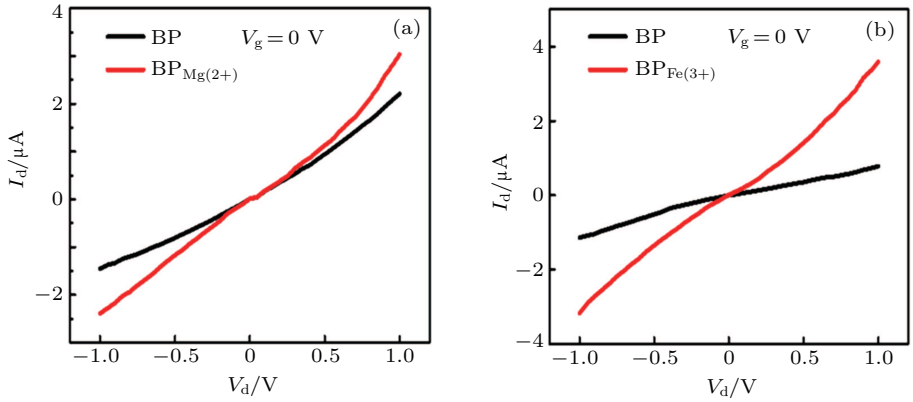


Fig. S7. (color online) I_{ds}–V_{ds} curve obtained from BP-FET devices on the Si/SiO_2 (300 nm) substrate before and after Mg^{2+} (a) and Fe^{3+} (b) adsorption for 60 s with concentration of 10^{-10} mol/L, at $V_g = 0$ V.

References

[1] Li L K, Yu Y J, Ye G J, Ge Q Q, Ou X D, Wu H, Feng D L, Chen X H and Zhang Y B 2014 *Nat. Nanotechnol.* **9** 372

[2] Liu H, Neal A T, Zhu Z, Luo Z, Xu X, Tomanek D and Ye P D 2014 *Acs Nano* **8** 4033

[3] Qiao J, Kong X, Hu Z X, Yang F and Ji W 2014 *Nat. Commun.* **5** 4475

[4] Yan S L, Xie Z J, Chen J H, Taniguchi T and Watanabe K 2017 *Chin. Phys. Lett.* **34** 047304

[5] Yu Y J and Zhang Y B 2017 *Physics* **46** 205 (in Chinese)

[6] Du Y, Liu H, Deng Y and Ye P D 2014 *Acs Nano* **8** 10035

[7] Zhu W, Yogeesh M N, Yang S, Aldave S H, Kim J S, Sonde S, Tao L, Lu N and Akinwande D 2015 *Nano Lett.* **15** 1883

[8] Saito Y and Iwasa Y 2015 *ACS Nano* **9** 3192

[9] Xiang D, Han C, Wu J, Zhong S, Liu Y, Lin J, Zhang X A, Hu W P, Oezyilmaz B, Castro Neto A H, Wee A T S and Chen W 2015 *Nat. Commun.* **6** 6485

[10] Qiao J S, Zhou L W and Ji W 2017 *Chin. Phys. B* **26** 036803

[11] Ren Y and Cheng F 2017 *Chin. Phys. Lett.* **34** 027302

[12] Xia F, Wang H and Jia Y 2014 *Nat. Commun.* **5** 4458

[13] Hong T, Chamlagain B, Lin W, Chuang H J, Pan M, Zhou Z and Xu Y Q 2014 *Nanoscale* **6** 8978

[14] Buscema M, Groenendijk D J, Blanter S I, Steele G A, van der Zant H S J and Castellanos-Gomez A 2014 *Nano Lett.* **14** 3347

[15] Ren X, Li Z, Huang Z, Sang D, Qiao H, Qi X, Li J, Zhong J and Zhang H 2017 *Adv. Funct. Mater.* **27** 1606834

[16] Guo Q, Pospischil A, Bhuiyan M, Jiang H, Tian H, Farmer D, Deng B, Li C, Han S J, Wang H, Xia Q, Ma T P, Mueller T and Xia F 2016 *Nano Lett.* **16** 4648

[17] Low T, Engel M, Steiner M and Avouris P 2014 *Phys. Rev. B* **90** 081408
[18] Wu J, Koon G K W, Xiang D, Han C, Toh C T, Kulkarni E S, Verzhbitskiy I, Carvalho A, Rodin A S, Koenig S P, Eda G, Chen W, Castro Neto A H and Oezyilmaz B 2015 *Acs Nano* **9** 8070
[19] Huang M, Wang M, Chen C, Ma Z, Li X, Han J and Wu Y 2016 *Adv. Mater.* **28** 3481
[20] Park C M and Sohn H J 2007 *Adv. Mater.* **19** 2465
[21] Sun J, Zheng G, Lee H W, Liu N, Wang H, Yao H, Yang W and Cui Y 2014 *Nano Lett.* **14** 4573
[22] Hu W, Lin L, Yang C, Dai J and Yang J 2016 *Nano Lett.* **16** 1675
[23] Guo Z, Zhang H, Lu S, Wang Z, Tang S, Shao J, Sun Z, Xie H, Wang H, Yu X F and Chu P K 2015 *Adv. Funct. Mater.* **25** 6996
[24] Sotor J, Sobon G, Macherzynski W, Paletko P and Abramski K M 2015 *Appl. Phys. Lett.* **107** 051108
[25] Ge Y, Chen S, Xu Y, He Z, Liang Z, Chen Y, Song Y, Fan D, Zhang K and Zhang H 2017 *J. Mater. Chem. C* **5** 6129
[26] Ismail E I, Kadir N A, Latiff A A, Ahmad H and Harun S W 2016 *Rsc Adv.* **6** 72692
[27] Sotor J, Sobon G, Kowalczyk M, Macherzynski W, Paletko P and Abramski K M 2015 *Opt. Lett.* **40** 3885
[28] Zhang B, Lou F, Zhao R, He J, Li J, Su X, Ning J and Yang K 2015 *Opt. Lett.* **40** 3691
[29] Park K, Lee J, Lee Y T, Choi W K, Lee J H and Song Y W 2015 *Annalen Der Physik* **527** 770
[30] Xing C, Chen S, Qiu M, Liang X, Liu Q, Zou Q, Li Z, Xie Z, Wang D, Dong B, Liu L, Fan D and Zhang H 2018 *Adv. Healthcare Mater.* **7** 1701510
[31] Qiu M, Wang D, Liang W, Liu L, Zhang Y, Chen X, Sang D K, Xing C, Li Z, Dong B, Xing F, Fan D, Bao S, Zhang H and Cao Y 2018 *Proc. Natl. Acad. Sci. USA* **115** 501
[32] Lu S, Ge Y, Sun Z, Huang Z, Cao R, Zhao C, Wen S, Fan D, Li J and Zhang H 2016 *Photon. Res.* **4** 286
[33] Xing C, Jing G, Liang X, Qiu M, Li Z, Cao R, Li X, Fan D and Zhang H 2017 *Nanoscale* **9** 8096
[34] Xu Y, Jiang X F, Ge Y, Guo Z, Zeng Z, Xu Q H, Zhang H, Yu X F and Fan D 2017 *J. Mater. Chem. C* **5** 3007
[35] Zheng J, Tang X, Yang Z, Liang Z, Chen Y, Wang K, Song Y, Zhang Y, Ji J, Liu Y, Fan D and Zhang H 2017 *Adv. Opt. Mater.* **5** Unsp 1700026
[36] Zheng J, Yang Z, Si C, Liang Z, Chen X, Cao R, Guo Z, Wang K, Zhang Y, Ji J, Zhang M, Fan D and Zhang H 2017 *ACS Photon.* **4** 1466
[37] Li X, Xiong X and Wu Y 2017 *Chin. Phys. B* **26** 037307
[38] Yang J and Lu Y 2017 *Chin. Phys. B* **26** 034201
[39] Hong Y, Zhang J and Zeng X C 2018 *Chin. Phys. B* **27** 036501
[40] Maryam A, Abbas G, Rashid M and Sattar A 2018 *Chin. Phys. B* **27** 017401
[41] Wang F Q 2017 *Chin. Phys. B* **26** 29
[42] Doganov R A, O'Farrell E C T, Koenig S P, Yeo Y, Ziletti A, Carvalho A, Campbell D K, Coker D F, Watanabe K, Taniguchi T, Castro Neto A H and Ozyilmaz B 2015 *Nat. Commun.* **6** 6647
[43] Favron A, Gaufres E, Fossard F, Phaneuf-L'Heureux A L, Tang N Y W, Levesque P L, Loiseau A, Leonelli R, Francoeur S and Martel R 2015 *Nat. Mater.* **14** 826
[44] Avsar A, Vera-Marun I J, Tan J Y, Watanabe K, Taniguchi T, Castro Neto A H and Oezyilmaz B 2015 *Acs Nano* **9** 4138
[45] Huang Y, Qiao J, He K, Bliznakov S, Sutter E, Chen X, Luo D, Meng F, Su D, Decker J, Ji W, Ruoff R S and Sutter P 2016 *Chem. Mater.* **28** 8330
[46] Edmonds M T, Tadich A, Carvalho A, Ziletti A, O'Donnell K M, Koenig S P, Coker D F, Oezyilmaz B, Castro Neto A H and Fuhrer M S 2015 *ACS Appl. Mater. & Interfaces* **7** 14557
[47] Guo Z, Chen S, Wang Z, Yang Z, Liu F, Xu Y, Wang J, Yi Y, Zhang H, Liao L, Chu P K and Yu X F 2017 *Adv. Mater.* **29** 1703811
[48] Whiteley C M, Valle M D, Jones K C and Sweetman A J 2013 *Environmental Sci.-Processes & Impacts* **15** 2050
[49] McGillicuddy E, Murray I, Kavanagh S, Morrison L, Fogarty A, Cormican M, Dockery P, Prendergast M, Rowan N and Morris D 2017 *Sci. Total Environ.* **575** 231
[50] Yang X, Jia Z, Yang X, Li G and Liao X 2017 *Saudi J. Biological Sci.* **24** 589
[51] Ramos K, Ramos L and Gomez-Gomez M M 2017 *Food Chem.* **221** 822
[52] Hallerstig L M, Granath P, Lindgren L and Tranberg M 2017 *Analytical Methods* **9** 149
[53] Lue P T, Huang X M, Lu Y M, Liu J P, Zhang Z Q and He S G 2011 *Spectroscopy and Spectral Analysis* **31** 2253
[54] Sugai S and Shirotani I 1985 *Solid State Commun.* **53** 753
[55] Ribeiro H B, Pimenta M A, de Matos C J S, Moreira R L, Rodin A S, Zapata J D, de Souza E A T and Castro Neto A H 2015 *ACS Nano* **9** 4270
[56] Wu J, Mao N, Xie L, Xu H and Zhang J 2015 *Angew. Chem.-Int. Ed.* **54** 2366